

# Quasicrystalline Altermagnetism

Rui Chen,<sup>1</sup> Bin Zhou,<sup>1</sup> and Dong-Hui Xu<sup>2,3,\*</sup>

<sup>1</sup>*Department of Physics, Hubei University, Wuhan 430062, China*

<sup>2</sup>*Department of Physics and Chongqing Key Laboratory for Strongly Coupled Physics, Chongqing University, Chongqing 400044, China*

<sup>3</sup>*Center of Quantum Materials and Devices, Chongqing University, Chongqing 400044, China*

Altermagnets are a recently discovered class of magnetic materials that combine a collinear, zero-magnetization spin structure, characteristic of antiferromagnets, with spin-split electronic bands, a hallmark of ferromagnets. This unique behavior arises from the breaking of combined time-reversal and spatial symmetries (such as inversion or lattice translation), which are preserved in conventional antiferromagnets. To date, research has focused on altermagnetic phases in periodic crystals, where the order is linked to specific crystallographic rotation symmetries. In this work, we demonstrate that quasicrystals, which possess rotational symmetries forbidden in periodic lattices, can host exotic altermagnetic orders. Using symmetry analysis and self-consistent mean-field theory, we predict stable *g*-wave and *i*-wave altermagnetism in octagonal and dodecagonal quasicrystals, respectively. These novel phases are characterized by global  $C_8T$  and  $C_{12}T$  symmetries and manifest as unique anisotropic spin-splittings in their spectral functions and spin conductance, featuring characteristic eight- and twelve-fold nodal structures that serve as unambiguous experimental fingerprints. Our findings establish quasicrystals as a versatile platform for realizing unconventional altermagnetic orders beyond the constraints of crystallographic symmetry.

**Introduction.**— Altermagnets represent a recently discovered class of magnetic materials, distinct from conventional ferromagnets and antiferromagnets [1–11]. They uniquely combine a collinear spin structure with zero net magnetization, characteristic of antiferromagnets, with spin-split electronic bands, a hallmark of ferromagnets. This unconventional behavior is rooted in the breaking of composite symmetries—specifically, time-reversal combined with spatial operations like inversion or translation—which remain intact in conventional antiferromagnets. It enables unique physical phenomena such as anomalous transport [12–16], giant tunneling magnetoresistance [17, 18], and potential topological responses [19–21], thereby prompting widespread research both theoretically and experimentally [22–28]. To date, however, the exploration of altermagnetism has been almost exclusively confined to periodic crystals. Within this paradigm, altermagnetic phases are protected by specific crystal rotational symmetries (e.g., four-fold or six-fold). This reliance on crystallographic symmetry fundamentally forbids altermagnets with higher-order or non-crystallographic rotational symmetries. This limitation necessitates the search for alternative platforms beyond conventional crystals to realize more exotic altermagnetic states.

Quasicrystals, with their long-range aperiodic order and ‘forbidden’ rotational symmetries, provide an ideal platform to transcend these crystalline constraints [29, 30]. While altermagnetism has been considered in amorphous systems lacking any long-range order [31], here we investigate a distinct paradigm where the altermagnetic order is protected by the global non-crystallographic rotational symmetries intrinsic to the long-range aperiodic

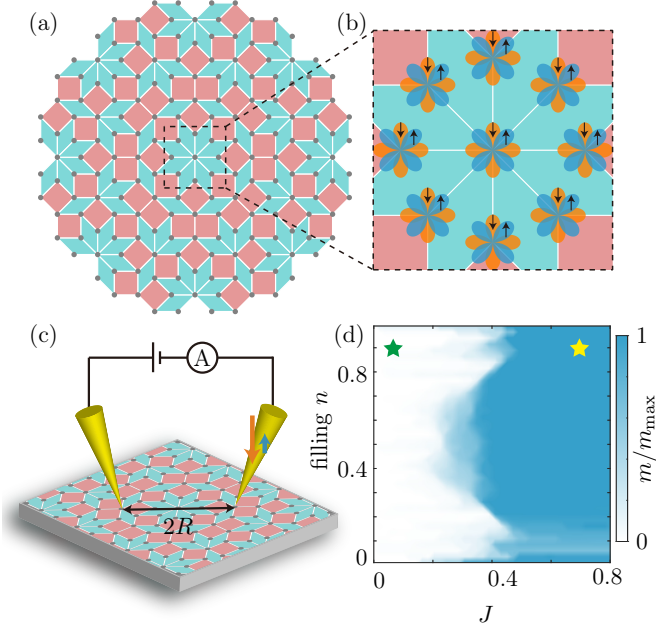


FIG. 1. (a) Schematic illustration of the AB-tiling octagonal quasicrystal, which consists of two types of primitive tiles: square tiles (red) and rhombus tiles (cyan) with an acute angle  $45^\circ$ . (b) Each site of the AB-tiling quasicrystal features two orbits (blue and orange) connected by a  $C_8$  rotation. (c) We propose that the altermagnetic order in quasicrystal can be probed by a double-tip STM setup. When a spin-unpolarized current is injected, the output current becomes spin-polarized due to the altermagnetic structure. (d) The normalized mean altermagnetization  $m/m_{\max}$  as a function of the filling  $n$  and the interaction coupling strength  $J$ . Each data point is obtained by using the self-consistent mean field method.

\* [donghuixu@cqu.edu.cn](mailto:donghuixu@cqu.edu.cn)

structure of quasicrystals. The potential for these materials to host complex magnetic states is no longer a purely theoretical possibility. Recent discoveries of ferromagnetism [32, 33] and antiferromagnetism [34, 35] in quasicrystals have demonstrated that their unique structures can support magnetic order. Most strikingly, the recent experimental observation of antiferromagnetism in the icosahedral quasicrystal  $\text{Au}_{56}\text{In}_{28.5}\text{Eu}_{15.5}$  [36] confirms that these symmetries can act as a protecting principle for novel, highly ordered magnetic states rather than inducing frustration. This confluence of theoretical possibility and experimental precedent makes quasicrystals a fertile ground for discovering new forms of magnetism.

In this work, we propose that quasicrystals can host altermagnetic phases with symmetries forbidden in any periodic crystal. Specifically, we show that the Ammann-Beenker (AB) tiling, a canonical octagonal quasicrystal, supports a  $g$ -wave altermagnetism protected by a composite eight-fold rotational symmetry  $C_8T$ , where  $T$  is time-reversal symmetry. Our analysis of the Fourier spectra reveals a momentum-dependent spin structure with a nodal  $g$ -wave configuration. We propose that this unique order can be detected via double-tip scanning tunneling microscopy (STM) [37–41] and show that transport measurements would exhibit a spin-polarized current whose anisotropy directly reflects the underlying  $g$ -wave symmetry. Furthermore, we extend our analysis to show that an  $i$ -wave altermagnetic phase can emerge in the Stampfli-tiling dodecagonal quasicrystal. Our findings establish a previously uncharted direction in magnetism, demonstrating that the rich symmetries of quasicrystals offer a new route to designing and discovering altermagnetic orders beyond the crystalline paradigm.

**Model.**—We adopt a minimal  $t$ - $J$ -like model for the orbital altermagnet phase in an AB-tiling quasicrystal [Fig. 1(a)]. The AB-tiling quasicrystal consists of two types of primitive tiles: square tiles (red) and rhombus tiles (cyan) with an acute angle of  $45^\circ$ . Each site contains two orbitals connected by a  $C_8$  rotation [Fig. 1(b)]. A concrete realization of this setup can be achieved with the  $d_{xy}$  and  $d_{x^2-y^2}$  orbitals, which naturally transform into each other under  $C_8$  rotations. The total Hamiltonian,  $H = H_K + H_{\text{Int}}$  [31], consists of a kinetic term and an interaction term. The kinetic term

$$H_K = \sum_{\langle jk \rangle} \Psi_j^\dagger [T(\eta\theta_{jk})] \sigma_0 \Psi_k, \quad (1)$$

describes hopping between adjacent sites. Here,  $\langle \dots \rangle$  denotes sites connected by the bonds of distance  $a = 1$ , as shown in Fig. 1(a).  $\Psi_j^\dagger = (c_{j\alpha\uparrow}^\dagger, c_{j\beta\uparrow}^\dagger, c_{j\alpha\downarrow}^\dagger, c_{j\beta\downarrow}^\dagger)$  are electron creation operators at site  $j$ .  $\alpha$  and  $\beta$  represent the two orbitals at one site and spin degrees of freedom are denoted as  $\uparrow$  and  $\downarrow$ .  $\theta_{jk}$  is the polar angle of bond connecting sites  $j$  and  $k$  with respect to the horizontal direction. The orbital-dependent hopping matrix is given

by

$$T(\eta\theta) = \begin{pmatrix} (t_1 - t_2) \cos^2 \eta\theta + t_2 & (t_1 - t_2) \sin \eta\theta \cos \eta\theta \\ (t_1 - t_2) \sin \eta\theta \cos \eta\theta & (t_1 - t_2) \sin^2 \eta\theta + t_2 \end{pmatrix}. \quad (2)$$

We fix  $t_1 = 1$ ,  $t_2 = 1/2$ , and  $\eta = 2$  in the case of the AB-tiling quasicrystal. At  $\theta = 0$ , the hopping is dominated by the overlap between the first orbitals  $t_1$ , while the second orbitals have a smaller overlap  $t_2$ , with  $t_2 < t_1$ . At  $\theta = \pi/4$ , these hopping strengths are reversed. This angular dependence captures the rotating orbital texture illustrated in Fig. 1(b), where the orbital character naturally twists along different bond directions due to the underlying  $C_8$  rotational symmetry.

We include a ferromagnetic Heisenberg-like combined spin-orbital interaction [31, 42]

$$H_{\text{Int}} = -J \sum_{\langle jk \rangle, \zeta\chi} (\Psi_j^\dagger \tau_\zeta \sigma_\chi \Psi_j) (\Psi_k^\dagger \tau_\zeta \sigma_\chi \Psi_k) - n_j n_k, \quad (3)$$

where  $n_j = \sum_{\mu,s} c_{j\mu s}^\dagger c_{j\mu s}$  is the total on-site occupation operator, with  $s = \uparrow, \downarrow$  labels spin and  $\mu = \alpha, \beta$  labels orbital.  $\sigma^\chi(\tau^\zeta)$  are Pauli matrices acting on the spin (orbital) subspace. In the single-fermion-per-site limit, Eq. (3) resembles a ferromagnetic Kugel-Khomskii interaction, expressed as  $(\mathbf{S}_j \cdot \mathbf{S}_k)(\boldsymbol{\tau}_j \cdot \boldsymbol{\tau}_k)$  [43].

**Mean Field Decoupling and the emergent altermagnetism.**—We employ an iterative, real-space Hartree-Fock mean-field method to determine the self-consistent ground state of the spin-orbital coupled system [31, 44, 45]. The interaction term is decoupled via a mean-field approximation, yielding an effective single-particle Hamiltonian

$$H_{\text{Int}} = -J \sum_{\langle jk \rangle} \langle m_j \rangle m_k - \langle n_j \rangle n_k + (j \leftrightarrow k), \quad (4)$$

where  $n_j$  is the total occupation and  $m_j = \Psi_j^\dagger \sigma^z \tau^z \Psi_j$  denotes the local magnetization. We assume spontaneous symmetry breaking occurs along the  $\sigma^z$  and orbital  $\tau^z$  directions, retaining only the diagonal components relevant to the symmetry-broken state. Due to the spin-rotational invariance of the interaction Hamiltonian, the resulting physical properties are independent of the chosen quantization axis for the emergent order. At each iteration, we compute site-resolved expectation values for the local charge density  $\langle n_j \rangle$  and magnetization  $\langle m_j \rangle$ . These expectation values are then used to update the mean-field Hamiltonian for the next iteration. This self-consistent procedure is repeated until convergence is achieved (typically within 200 iterations) and allows for spatially inhomogeneous ordering without presupposing translational symmetry.

This interaction term in Eq. (4) lifts the degeneracy among the four spin-orbital configurations. For a positive  $m_j$ , the states  $|\alpha \uparrow\rangle$  and  $|\beta \downarrow\rangle$  on the  $j$ -th site have lower energy, whereas  $|\beta \uparrow\rangle$  and  $|\alpha \downarrow\rangle$  have higher energy. Consequently, the spin and orbital degrees of free-

dom become locked, with electrons in the  $\alpha$ -orbital predominantly carrying spin-up and those in the  $\beta$ -orbital carrying spin-down [see Fig. 1(b)]. This establishes the altermagnetic phase in quasicrystals. Although the magnetic term  $m_j$  individually breaks the eightfold rotation symmetry  $C_8 = \tau_x \sigma_0 \mathcal{R}_8$  and time-reversal symmetry  $T = i\tau_0 \sigma_y \mathcal{K}$ , their combination  $C_8 T$ , remains a preserved symmetry of the system. Here,  $\mathcal{R}_8$  is the orthogonal matrix that permutes the tiling sites to rotate the whole system by  $\pi/4$  and  $\mathcal{K}$  is complex conjugation. This composite symmetry plays a central role in characterizing the altermagnetic phase.

**Interaction-induced altermagnetic ordering.**—Figure 1(d) presents the averaged magnetization normalized by its maximal value,  $m/m_{\max}$ , as a function of the filling  $n$  and the interaction coupling strength  $J$ . The average magnetization is defined as  $m = \sum_j \langle m_j \rangle / N$ , where  $N = 833$  is the total number of lattice sites. The normalization factor  $m_{\max} = 2 - |4n - 2|$  represents the theoretical upper bound derived from the occupation constraints [31]. For small  $J$ , the system settles into a trivial metallic state, as the local altermagnetization  $\langle m_j \rangle$  vanishes during the self-consistent calculation. For larger  $J$ , a stable altermagnetic phase emerges with a finite order parameter  $m$ , which approaches its theoretical maximum  $m/m_{\max} \rightarrow 1$  in the strong-coupling regime.

**Spectral Function.**—Direct visualization of spin-resolved momentum-space textures is experimentally challenging but has become increasingly feasible, even for complex materials like quasicrystals, thanks to the development of high-efficiency, multichannel spin detectors. Although quasicrystals lack discrete translational symmetry, meaning crystal momentum is not a good quantum number, their momentum-space properties can still be probed via Fourier analysis. Specifically, one can project eigenstates onto plane-wave-like trial states of the form:  $|\mathbf{ps}\mu\rangle = N \sum_{\mathbf{x}_j} e^{i\mathbf{p}\cdot\mathbf{x}_j} |\mathbf{x}_j s\mu\rangle$ . These trial states serve as Fourier components of the real-space basis, representing spatial modulations with wave vector  $\mathbf{p}$ . This Fourier-based projection thus provides a practical framework for analyzing the momentum-space structure of quasicrystalline systems in the absence of a Brillouin zone [46, 47]. We therefore compute the spin-resolved spectral function [31]

$$\mathcal{A}_s(\mathbf{p}) = -\frac{\eta}{\pi} \sum_{\lambda\mu} \frac{|\langle \lambda | \mathbf{ps}\mu \rangle|^2}{(\varepsilon_F - \varepsilon_\lambda)^2 + \eta^2}, \quad (5)$$

where  $\eta$  is a small broadening factor and  $\varepsilon_F$  is the Fermi level corresponding to the filling number  $n$ . This quantity is directly accessible in spin-resolved angle-resolved photoemission spectroscopy (ARPES) measurements on quasicrystalline samples [48, 49].

Figures 2(a)-2(b) show the numerically calculated spectra with  $J = 0.05$  [marked by the green star in Fig. 1(d)]. For this weak coupling, the system remains a trivial metal, and the spin-up and spin-down spectral functions are degenerate. The spectrum exhibits

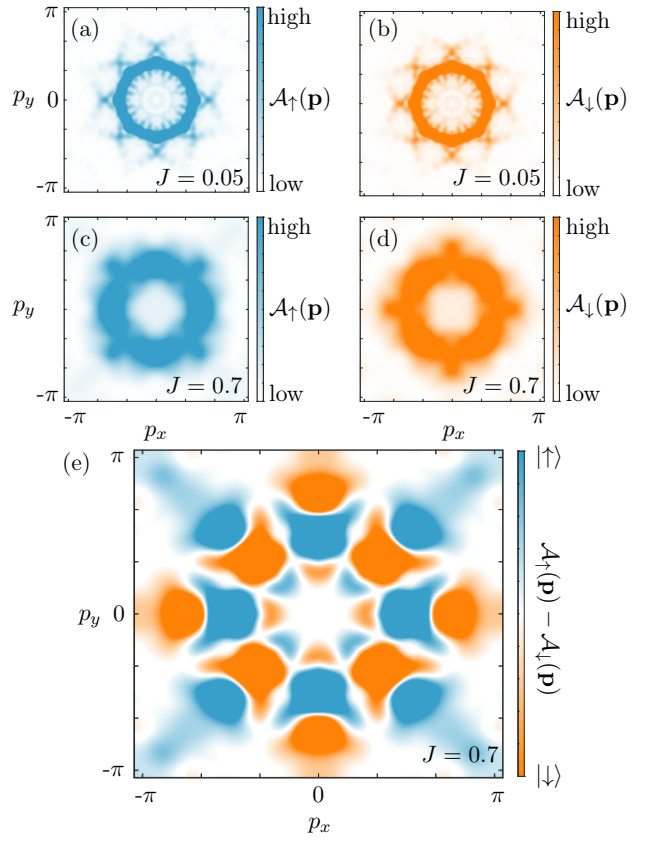


FIG. 2. Spectral density  $\mathcal{A}(\mathbf{p})$  as a function of momentum  $\mathbf{p}$ . (a) and (c) show the spin-up spectral density  $\mathcal{A}_\uparrow(\mathbf{p})$ . (b) and (d) show the spin-down spectral density  $\mathcal{A}_\downarrow(\mathbf{p})$ . (e) presents the spin-resolved difference  $\mathcal{A}_\uparrow(\mathbf{p}) - \mathcal{A}_\downarrow(\mathbf{p})$ . We take the interaction coupling  $J = 0.05$  in (a) and (b), and  $J = 0.7$  in (c)-(e). The electron filling is fixed at  $n = 0.9$  in all panels.

an eightfold rotational symmetry, reflecting the underlying symmetry of the quasicrystal lattice. The system also features a fractal-like spectral pattern, reflecting the fractal nature of the quasicrystals [50, 51].

Figures 2(c)-2(d) show the spectra for a strong interaction coupling of  $J = 0.7$  [marked by the yellow star in Fig. 1(d)]. In this regime, the system enters an altermagnetic phase, characterized by a finite self-consistent altermagnetic order. This results in a clear spin splitting in the spectral functions, accompanied by the breaking of  $C_8$  symmetry while preserving a residual  $C_4$  symmetry. Crucially, the spin-up and spin-down spectral functions are related by a  $C_8$  rotation due to the preserved  $C_8 T$  symmetry of the whole system. Consequently, the difference  $\mathcal{A}_\uparrow(\mathbf{p}) - \mathcal{A}_\downarrow(\mathbf{p})$  transforms antisymmetrically under a  $C_8$  rotation, meaning it changes sign and must vanish along the nodal line defined by  $\theta = \pi/8 + n\pi/4$ .

**Spin-Conductance.**—Another distinguishing experimental feature of altermagnetism is its unique spin transport properties [12–18]. We employ the two-terminal device to investigate the transport properties of the quasicrystalline system, where each lead is modeled

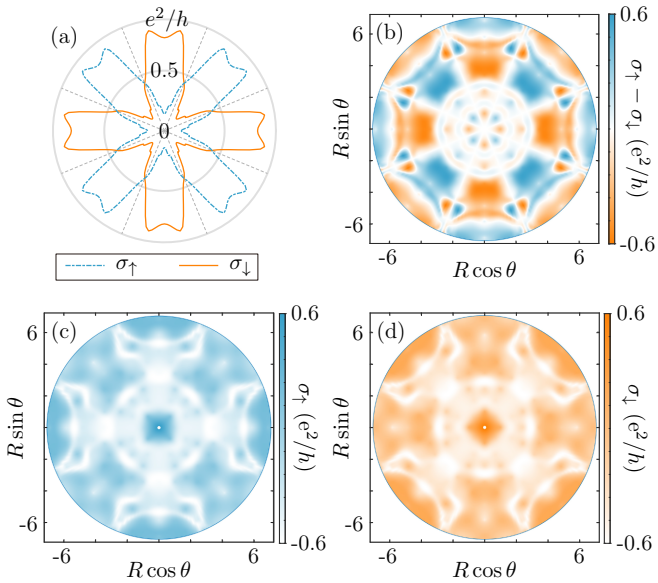


FIG. 3. (a) Spin conductances  $\sigma_\uparrow$  and  $\sigma_\downarrow$  as functions of the angle  $\phi$  with  $R = 4$ . (b)  $\sigma_\uparrow - \sigma_\downarrow$  as functions of the angle  $\phi$  and the radius  $R$ . (c) and (d) depict the  $\sigma_\uparrow$  and  $\sigma_\downarrow$  as functions of the angle  $\phi$  and the radius  $R$ . We take  $J = 0.7$  and  $n = 0.9$  in all panels.

as a scanning STM tip. One tip is positioned at  $R(\cos\phi, \sin\phi)$ , and the other is symmetrically located at  $-R(\cos\phi, \sin\phi)$ . By varying the probe separation  $R$  and angle  $\phi$ , the setup allows angle-resolved probing of the transport anisotropy.

Specifically, each STM tip is modeled as a one-dimensional chain with the Hamiltonian  $H_{\text{tip}} = \sum_{\langle jk \rangle} \Phi_j^\dagger t \tau_0 \sigma_0 \Phi_k$ , where  $\Phi_j$  denotes the spinor at site  $j$  in the lead and  $t = 1$ . The coupling between the tip and the device is described by the tunneling Hamiltonian  $H' = \sum_{jk} \Psi_j^\dagger t e^{-r_{jk}} \tau_0 \sigma_0 \Phi_k + \text{h.c.}$ , where  $\Psi_j$  denotes the spinor on the device [see Eq. (1)], and  $r_{jk}$  is the distance between the device site  $j$  and the lead site  $k$ . The exponential factor ensures that the coupling is spatially localized, restricting the tunneling to sites in close proximity to the tip position. The conductance between the two tips is calculated by using the Landauer-Büttiker formula [52–54] and the recursive Green's function method [55, 56].

Figure 3(a) shows the spin conductance  $\sigma_{\uparrow,\downarrow}$  as functions of angle  $\phi$  for  $R = 4$ . The spin-dependent conductance exhibits strong anisotropy, a phenomenon more clearly visualized in Figs. 3(c)-(d), where we plot  $\sigma_{\uparrow,\downarrow}$  as functions of  $R \cos \theta$  and  $R \sin \theta$ . Similar to the spectral function, the conductance for each spin component displays a clear  $C_4$  symmetry. However, a  $C_8$  rotation transforms the spin-up conductance into the spin-down conductance. As a result, the difference  $\sigma_\uparrow - \sigma_\downarrow$  changes sign under an eight-fold rotation and must vanish along the nodal line  $\theta = \pi/8 + n\pi/4$  [see Fig. 3(b)]. These trans-

port signatures further confirm that the system realizes a  $g$ -wave altermagnet. While experimentally demanding, multi-probe STM techniques provide a unique and powerful route to probe non-local transport anisotropies and correlation functions. Our calculations thus provide a clear theoretical target and a strong motivation for such advanced measurements, where the predicted symmetry of the spin-conductance offers an unambiguous signature of the underlying quasicrystalline altermagnetic order.

*Stampfli-tiling dodecagonal quasicrystals.*—We extend our analysis to the Stampfli-tiling quasicrystal [Fig. 4(a)], which features a global twelve-fold rotational symmetry [48]. This tiling consists of three primitive tiles: squares (red), regular triangles (purple), and rhombuses (cyan) with an acute angle of  $30^\circ$ . The Hamiltonian is analogous to the AB-tiling case, but with  $\eta = 3$  in Eqs. (1)-(2) to reflect the  $C_{12}$  symmetry. This can be realized by choosing the  $f_{x(x^2-3y^2)}$  and  $f_{y(3x^2-y^2)}$  orbitals. In this setup, for  $\theta = 0$ , hopping is dominated by the overlap  $t_1$  between the first orbitals and the second orbital have a smaller overlap  $t_2$  [Figs. 4(a)-4(b)]. For  $\theta = \pi/6$ , the roles are reversed.

Figure 4(f) shows the normalized altermagnetization  $m/m_{\max}$  as a function of filling  $n$  and interaction coupling strength  $J$ . We find that the altermagnetic phase in the Stampfli-tiling quasicrystal remains stable at large  $J$ , with  $m$  approaching its theoretical maximum. This behavior closely resembles our findings for the AB-tiling quasicrystal, indicating that the emergence of altermagnetism is a robust feature in quasicrystalline systems with high-fold rotational symmetries.

Figures 4(c)-4(e) and 4(g)-4(h) present the spectral functions and transport properties of the Stampfli-tiling system, respectively. Due to the underlying  $C_{12}$  symmetry, the spin-up and spin-down components of the spectra and transport response are related by a twelve-fold rotation. As a result, their differences, i.e.,  $A_\uparrow(\mathbf{p}) - A_\downarrow(\mathbf{p})$  and  $\sigma_\uparrow - \sigma_\downarrow$ , exhibit antisymmetric behavior under  $C_{12}$  rotations, changing sign upon a  $\pi/6$  rotation. These signatures establish the presence of a  $C_{12}T$  protected  $i$ -wave altermagnetic phase in this quasicrystal.

*Conclusion.*—We have extended the concept of altermagnetism to quasicrystals, demonstrating that their unique high-fold rotational symmetries, forbidden in periodic crystals, can protect novel altermagnetic phases. By calculating symmetry-protected spectral textures and transport features, we have identified clear experimental signatures. The characteristic spectral textures are directly accessible via spin-resolved ARPES, and the anisotropic transport signatures can be probed using multi-tip STM. The proposed detection schemes provide a realistic route toward observing and confirming these exotic altermagnetic phases in quasicrystals.

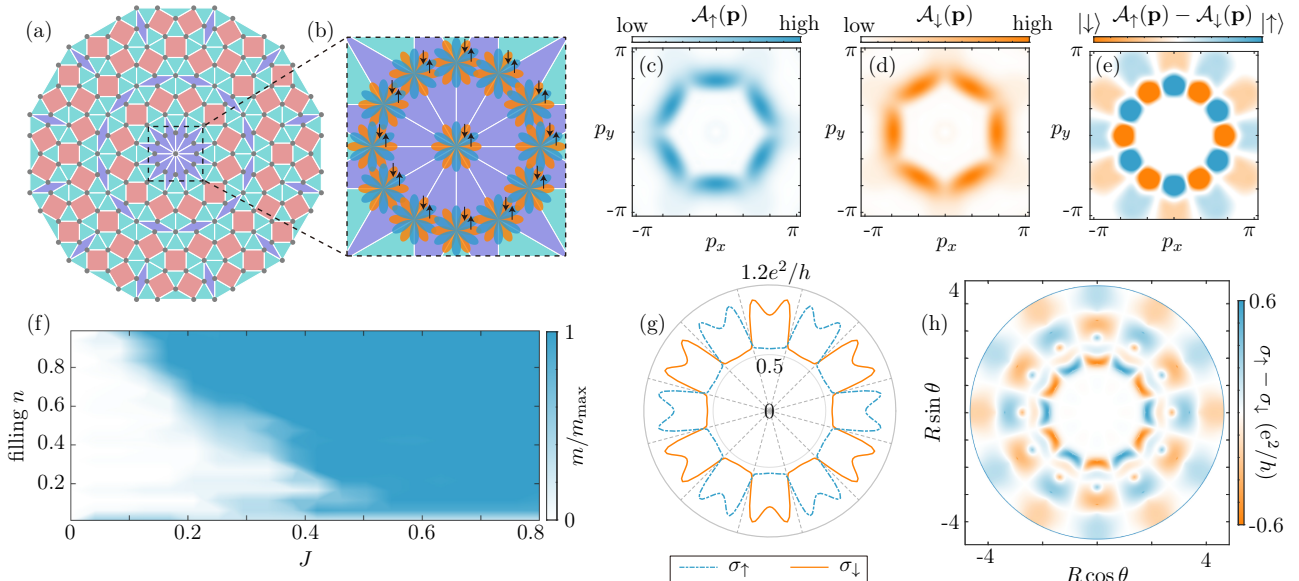


FIG. 4. (a) Schematic illustration of the Stampfli-tiling dodecagonal quasicrystals. (b) Each site of the Stampfli-tiling quasicrystal features two orbits connected by a  $C_{12}$  rotation. (c) The normalized mean altermagnetization  $m/m_{\max}$  as a function of the filling  $n$  and the interaction coupling strength  $J$ . (e), (f), and (g) describes the  $\mathcal{A}_\uparrow(\mathbf{p})$ ,  $\mathcal{A}_\downarrow(\mathbf{p})$ , and  $\mathcal{A}_\uparrow(\mathbf{p}) - \mathcal{A}_\downarrow(\mathbf{p})$ , respectively. (h) Spin conductances  $\sigma_\uparrow$  and  $\sigma_\downarrow$  as functions of the angle  $\phi$  with  $R = 4$ . (i)  $\sigma_\uparrow - \sigma_\downarrow$  as functions of the angle  $\phi$  and the radius  $R$ . The electron filling is fixed at  $n = 0.9$  in (c)-(e) and (g)-(h).

## ACKNOWLEDGMENTS

D.-H.X. was supported by the NSFC (under Grants Nos. 12474151, 12074108, and 12347101) and Beijing National Laboratory for Condensed Matter Physics (No. 2024BNLCMPKF025). R.C. acknowledges the support of the NSFC (under Grant No. 12304195), the Chutian Scholars Program in Hubei Province, the Hubei Provincial Natural Science Foundation (Grant

No. 2025AFA081), and the original seed program of Hubei University. B.Z. was supported by the NSFC (under Grant No. 12074107), the program of outstanding young and middle-aged scientific and technological innovation team of colleges and universities in Hubei Province (under Grant No. T2020001) and the innovation group project of the natural science foundation of Hubei Province of China (under Grant No. 2022CFA012).

- 
- [1] L. Šmejkal, J. Sinova, and T. Jungwirth, “Beyond conventional ferromagnetism and antiferromagnetism: A phase with nonrelativistic spin and crystal rotation symmetry”, *Phys. Rev. X* **12**, 031042 (2022).
- [2] L. Bai, W. Feng, S. Liu, L. Šmejkal, Y. Mokrousov, and Y. Yao, “Altermagnetism: Exploring new frontiers in magnetism and spintronics”, *Adv. Funct. Mater.* , **24**09327 (2024).
- [3] M. Naka, S. Hayami, H. Kusunose, Y. Yanagi, Y. Motome, and H. Seo, “Spin current generation in organic antiferromagnets”, *Nat. Commun.* **10**, 4305 (2019).
- [4] K.-H. Ahn, A. Hariki, K.-W. Lee, and J. Kuneš, “Antiferromagnetism in RuO<sub>2</sub> as *d*-wave Pomeranchuk instability”, *Phys. Rev. B* **99**, 184432 (2019).
- [5] S. Hayami, Y. Yanagi, and H. Kusunose, “Momentum-dependent spin splitting by collinear antiferromagnetic ordering”, *J. Phys. Soc. Jpn.* **88**, 123702 (2019).
- [6] L.-D. Yuan, Z. Wang, J.-W. Luo, E. I. Rashba, and A. Zunger, “Giant momentum-dependent spin splitting in centrosymmetric low-*z* antiferromagnets”, *Phys. Rev.*
- [7] I. I. Mazin, K. Koepernik, M. D. Johannes, R. González-Hernández, and L. Šmejkal, “Prediction of unconventional magnetism in doped FeSb<sub>2</sub>”, *Proc. Nat. Acad. Sci.* **118**, e2108924118 (2021).
- [8] H.-Y. Ma, M. Hu, N. Li, J. Liu, W. Yao, J.-F. Jia, and J. Liu, “Multifunctional antiferromagnetic materials with giant piezomagnetism and noncollinear spin current”, *Nat. Commun.* **12**, 2846 (2021).
- [9] L. Šmejkal, J. Sinova, and T. Jungwirth, “Emerging research landscape of altermagnetism”, *Phys. Rev. X* **12**, 040501 (2022).
- [10] J. Krempaský, L. Šmejkal, S. D’souza, M. Hajlaoui, G. Springholz, K. Uhlířová, *et al.*, “Altermagnetic lifting of kramers spin degeneracy”, *Nature* **626**, 517 (2024).
- [11] L. Šmejkal, A. H. MacDonald, J. Sinova, S. Nakatsuji, and T. Jungwirth, “Anomalous Hall antiferromagnets”, *Nat. Rev. Mat.* **7**, 482 (2022).
- [12] M. Naka, Y. Motome, and H. Seo, “Perovskite as a spin current generator”, *Phys. Rev. B* **103**, 125114 (2021).

- [13] D.-F. Shao, S.-H. Zhang, M. Li, C.-B. Eom, and E. Y. Tsymbal, “Spin-neutral currents for spintronics”, *Nat. Commun.* **12**, 7061 (2021).
- [14] R. M. Fernandes, V. S. de Carvalho, T. Birol, and R. G. Pereira, “Topological transition from nodal to nodeless zeeman splitting in altermagnets”, *Phys. Rev. B* **109**, 024404 (2024).
- [15] R.-W. Zhang, C. Cui, R. Li, J. Duan, L. Li, Z.-M. Yu, and Y. Yao, “Predictable gate-field control of spin in altermagnets with spin-layer coupling”, *Phys. Rev. Lett.* **133**, 056401 (2024).
- [16] X. Zhou, W. Feng, R.-W. Zhang, L. Šmejkal, J. Sinova, Y. Mokrousov, and Y. Yao, “Crystal Thermal Transport in Altermagnetic RuO<sub>2</sub>”, *Phys. Rev. Lett.* **132**, 056701 (2024).
- [17] H. Li, G. Wang, N. Ding, Q. Ren, G. Zhao, W. Lin, *et al.*, “Spectroscopic evidence of spin-state excitation in d-electron correlated semiconductor FeSb<sub>2</sub>”, *Proc. Nat. Acad. Sci.* **121**, e2321193121 (2024).
- [18] L. Šmejkal, A. B. Hellenes, R. González-Hernández, J. Sinova, and T. Jungwirth, “Giant and tunneling magnetoresistance in unconventional collinear antiferromagnets with nonrelativistic spin-momentum coupling”, *Phys. Rev. X* **12**, 011028 (2022).
- [19] M. Ezawa, “Detecting the Néel vector of altermagnets in heterostructures with a topological insulator and a crystalline valley-edge insulator”, *Phys. Rev. B* **109**, 245306 (2024).
- [20] Y.-X. Li, Y. Liu, and C.-C. Liu, “Creation and manipulation of higher-order topological states by altermagnets”, *Phys. Rev. B* **109**, L201109 (2024).
- [21] R. Chen, Z.-M. Wang, H.-P. Sun, B. Zhou, and D.-H. Xu, “Probing *k*-space alternating spin polarization via the anomalous hall effect”, *arXiv:2501.14217* (2025).
- [22] H. Bai, Y. C. Zhang, Y. J. Zhou, P. Chen, C. H. Wan, L. Han, *et al.*, “Efficient spin-to-charge conversion via altermagnetic spin splitting effect in antiferromagnet ruo<sub>2</sub>”, *Phys. Rev. Lett.* **130**, 216701 (2023).
- [23] R. González-Hernández, L. Šmejkal, K. Výborný, Y. Yaghgi, J. Sinova, T. c. v. Jungwirth, and J. Železný, “Efficient electrical spin splitter based on nonrelativistic collinear antiferromagnetism”, *Phys. Rev. Lett.* **126**, 127701 (2021).
- [24] L. Šmejkal, R. González-Hernández, T. Jungwirth, and J. Sinova, “Crystal time-reversal symmetry breaking and spontaneous Hall effect in collinear antiferromagnets”, *Sci. Adv.* **6**, eaaz8809 (2020).
- [25] Z. Feng, X. Zhou, L. Šmejkal, L. Wu, Z. Zhu, H. Guo, *et al.*, “An anomalous Hall effect in altermagnetic ruthenium dioxide”, *Nat. Elec.* **5**, 735 (2022).
- [26] O. Fedchenko, J. Minar, A. Akashdeep, S. W. DSouza, D. Vasilyev, O. Tkach, *et al.*, “Observation of time-reversal symmetry breaking in the band structure of altermagnetic RuO<sub>2</sub>”, *Sci. Adv.* **10**, eadg4883 (2024).
- [27] S. Karube, T. Tanaka, D. Sugawara, N. Kadoguchi, M. Kohda, and J. Nitta, “Observation of Spin-Splitter Torque in Collinear Antiferromagnetic RuO<sub>2</sub>”, *Phys. Rev. Lett.* **129**, 137201 (2022).
- [28] P. Keßler, L. Garcia-Gassull, A. Suter, T. Prokscha, Z. Salman, D. Khalyavin, *et al.*, “Absence of magnetic order in RuO<sub>2</sub>: insights from  $\mu$ SR spectroscopy and neutron diffraction”, *npj Spintronics* **2**, 50 (2024).
- [29] B. Grünbaum and G. C. Shephard, *Tilings and patterns* (Courier Dover Publications, 1987).
- [30] W. Steurer and S. Deloudi, “Fascinating quasicrystals”, *Acta Crystallographica Section A Foundations of Crystallography* **64**, 1–11 (2007).
- [31] P. d’Ornellas, V. Leeb, A. G. Grushin, and J. Knolle, “Altermagnetism without crystal symmetry”, *arXiv:2504.08597* (2025).
- [32] R. Takeuchi, F. Labib, T. Tsugawa, Y. Akai, A. Ishikawa, S. Suzuki, T. Fujii, and R. Tamura, “High phase-purity and composition-tunable ferromagnetic icosahedral quasicrystal”, *Phys. Rev. Lett.* **130**, 176701 (2023).
- [33] R. Tamura, A. Ishikawa, S. Suzuki, T. Kotajima, Y. Tanaka, T. Seki, *et al.*, “Experimental observation of long-range magnetic order in icosahedral quasicrystals”, *J. Am. Chem. Soc.* **143**, 19938–19944 (2021).
- [34] S. Wessel, A. Jagannathan, and S. Haas, “Quantum antiferromagnetism in quasicrystals”, *Phys. Rev. Lett.* **90**, 177205 (2003).
- [35] F. Labib, T. Sugimoto, H. Takakura, A. Ishikawa, and R. Tamura, “Identification of two distinct antiferromagnetic phases in the au-al-gd quasicrystal approximant”, *Phys. Rev. B* **111**, 174409 (2025).
- [36] R. Tamura, T. Abe, S. Yoshida, Y. Shimozaki, S. Suzuki, A. Ishikawa, *et al.*, “Observation of antiferromagnetic order in a quasicrystal”, *Nat. Phys.* , 974 (2025).
- [37] M. Leeuwenhoek, F. Groenewoud, K. van Oosten, T. Benschop, M. P. Allan, and S. Groblacher, “Fabrication of on-chip probes for double-tip scanning tunneling microscopy”, *Microsystems Nanoengineering* **6**, 99 (2020).
- [38] A. Matsui and Y. Shigeta, “Development of probe-to-probe approach method for an independently controlled dual-probe scanning tunneling microscope”, *Rev. Sci. Instrum.* **78**, 106107 (2007).
- [39] T. Nakanishi and T. Ando, “Conductance images between two STM probes in graphene”, *Phys. E: Low-Dimens. Syst. Nanostructures* **42**, 726–728 (2010).
- [40] S. M. Hus, X.-G. Zhang, G. D. Nguyen, W. Ko, A. P. Baddorf, Y. P. Chen, and A.-P. Li, “Detection of the spin-chemical potential in topological insulators using spin-polarized four-probe STM”, *Phys. Rev. Lett.* **119**, 137202 (2017).
- [41] Y. Su, G. Zhang, D. Cao, and C. Zhang, “Coincidence double-tip scanning tunneling spectroscopy”, *arXiv:2507.17532* (2025).
- [42] S. Giuli, C. Mejuto-Zaera, and M. Capone, “Altermagnetism from interaction-driven itinerant magnetism”, *Phys. Rev. B* **111**, L020401 (2025).
- [43] K. I. Kugel and D. I. Khomskii, “The Jahn-Teller effect and magnetism: transition metal compounds”, *Soviet Physics Uspekhi* **25**, 231–256 (1982).
- [44] L. Classen, A. V. Chubukov, C. Honerkamp, and M. M. Scherer, “Competing orders at higher-order van hove points”, *Phys. Rev. B* **102**, 125141 (2020).
- [45] N. Lanatà, “Operatorial formulation of the ghost rotationally invariant slave-boson theory”, *Phys. Rev. B* **105**, 045111 (2022).
- [46] O. Lesser and R. Lifshitz, “Emergence of quasiperiodic bloch wave functions in quasicrystals”, *Phys. Rev. Res.* **4**, 013226 (2022).
- [47] D. Varjas, A. Lau, K. Pöyhönen, A. R. Akhmerov, D. I. Pikulin, and I. C. Fulga, “Topological phases without crystalline counterparts”, *Phys. Rev. Lett.* **123**, 196401 (2019).
- [48] S. J. Ahn, P. Moon, T.-H. Kim, H.-W. Kim, H.-C. Shin,

- E. H. Kim, *et al.*, “Dirac electrons in a dodecagonal graphene quasicrystal”, *Science* **361**, 782–786 (2018).
- [49] V. A. Rogalev, O. Gröning, R. Widmer, J. H. Dil, F. Bisti, L. L. Lev, T. Schmitt, and V. N. Strocov, “Fermi states and anisotropy of brillouin zone scattering in the decagonal al–ni–co quasicrystal”, *Nat. Commun.* **6** (2015), 10.1038/ncomms9607.
- [50] A. Jagannathan, “The fibonacci quasicrystal: Case study of hidden dimensions and multifractality”, *Rev. Mod. Phys.* **93**, 045001 (2021).
- [51] M. A. Bandres, M. C. Rechtsman, and M. Segev, “Topological photonic quasicrystals: Fractal topological spectrum and protected transport”, *Phys. Rev. X* **6**, 011016 (2016).
- [52] R. Landauer, “Electrical resistance of disordered one-dimensional lattices”, *Philos. Mag.* **21**, 863 (1970).
- [53] M. Büttiker, “Absence of backscattering in the quantum Hall effect in multiprobe conductors”, *Phys. Rev. B* **38**, 9375 (1988).
- [54] D. S. Fisher and P. A. Lee, “Relation between conductivity and transmission matrix”, *Phys. Rev. B* **23**, 6851 (1981).
- [55] A. MacKinnon, “The calculation of transport properties and density of states of disordered solids”, *Z. Phys. B* **59**, 385 (1985).
- [56] G. Metalidis and P. Bruno, “Green’s function technique for studying electron flow in two-dimensional mesoscopic samples”, *Phys. Rev. B* **72**, 235304 (2005).